Supplementary Materials

Molecular Layer Deposition of Biomimetic Amino Acid-based Hybrid Thin Films for Artificial Nociceptor

Lin Zhu,[1] Chu-Yi Zhang,[1] Li Gao,[1,3] Li-Ling Fu,[1] Chen Wang,[1] Yan-Qiang Cao[2], Wei-Min Li,[1,3] and Ai-Dong Li[1]*

[1]National Laboratory of Solid State Microstructures, Materials Science and Engineering Department, College of Engineering and Applied Sciences, Collaborative Innovation Center of Advanced Microstructures, Nanjing University, Nanjing 210093, P. R. China, Email: adli@nju.edu.cn

[2]School of Science, Nanjing University of Science and Technology, Nanjing 210094, P. R. China

[3]Jiangsu Leadmicro Nano-Technology Co., Ltd., Wuxi, Jiangsu, People's Republic of China

The thickness of Ti-Cys hybrid films was measured using both *ex situ* spectroscopic ellipsometry and cross-section SEM image. The cross-sectional SEM image of the 800-cycle hybrid film is presented in Figure S1, in consistent with the result of spectroscopic ellipsometry.

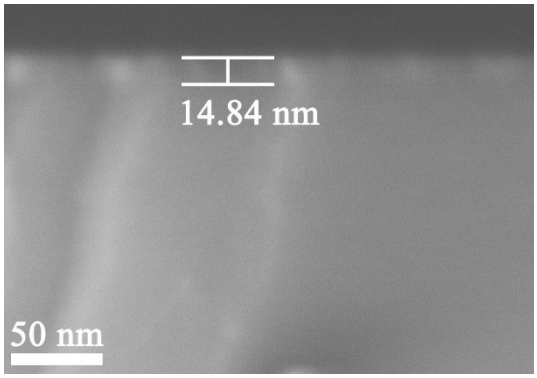

Fig. S1 Cross-sectional SEM image of the Ti-Cys hybrid film for 800-cycle sample deposited at 135 ℃.

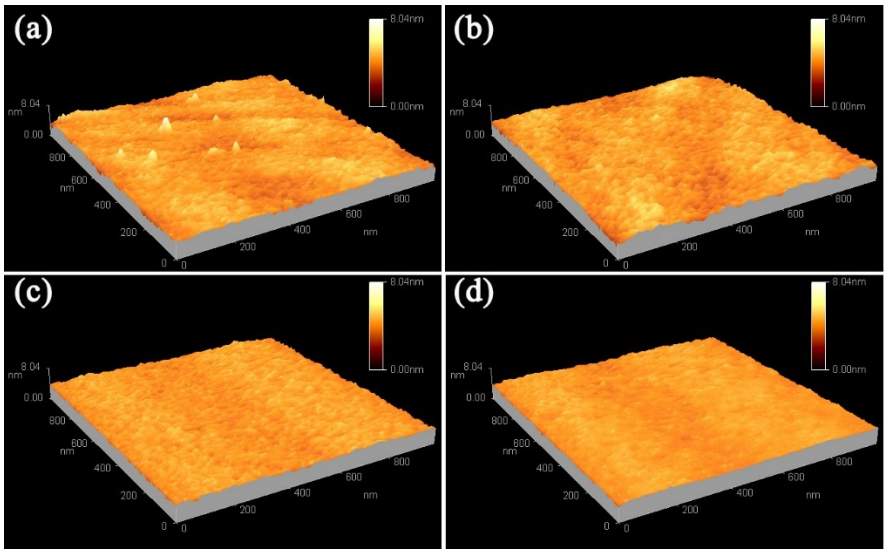

Fig. S2 AFM images (1 μm×1 μm) for Ti-Cys hybrid films deposited at (a) 175 ℃, (b) 200 ℃, (c) 220 ℃ and (d) 250 ℃.

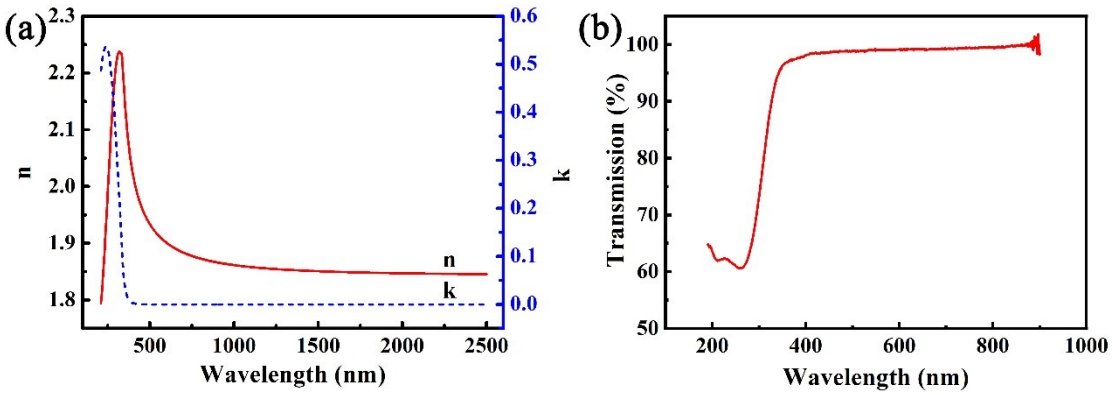

Fig. S3 (a) Refractive index (n) and extinction coefficient (k) versus wavelength, (b) UV–Vis transmitted spectra for the 200 cycles Ti-Cys hybrid film grown at 135 ℃.

XRD pattern of Ti-Cys hybrid film shows only one diffraction peaks at 2θ=28.2°, corresponding to the Si(111) from the substrate. No other peaks can be observed.

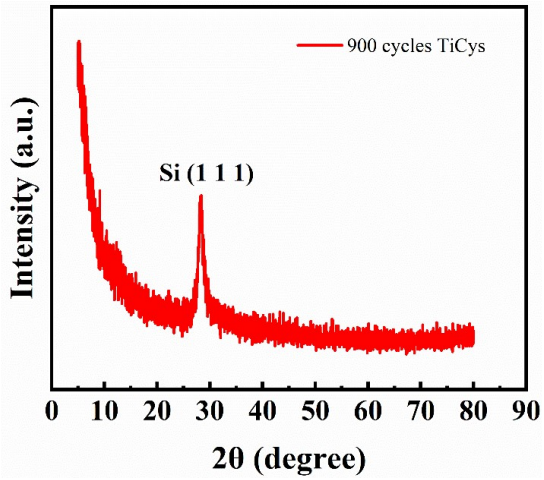

Fig. S4 XRD pattern of the Ti-Cys hybrid film.

Table S1 Assignment of bands found of L-cysteine and Ti-Cys hybrid films.

Wavenumber/cm^{-1}		Assignment*
L-Cys	Ti-Cys	
671	671	**CS str.**
776	776	**CH_2 rock.**
832	832	**COO wagg.**
866	866	**CCstr.**
988		**SH bend.**
1060	1080	**NH_3 rock.**
1100	1100	**CH bend.**
1201		**CH_2 twist.**
1219		**CH_2 twist.**
1326		**CHrock.**
1400	1418	**CH_2 bend.**
1425	1454	**CH_2 bend.**
1488		**CH_2 bend.**
1577	1571	**NH_3 bend. asym.**
1717		**COO str. asym.**
2551		**SH str.**
2605		**SH str.**
2686		**SH str.**
3280		**NH_3 str. asym.**
3425		**OH str.**

* str.=stretching, rock.=rocking, wagg.=wagging, bend.=bending, twist.=twisting,

sym.=symmetric, asym.=asymmetric.

AFM and SEM images indicate that the morphology of the Ti-Cys hybrid films does not change after exposure to air or water, as shown in Figure 8 and Figure S5.

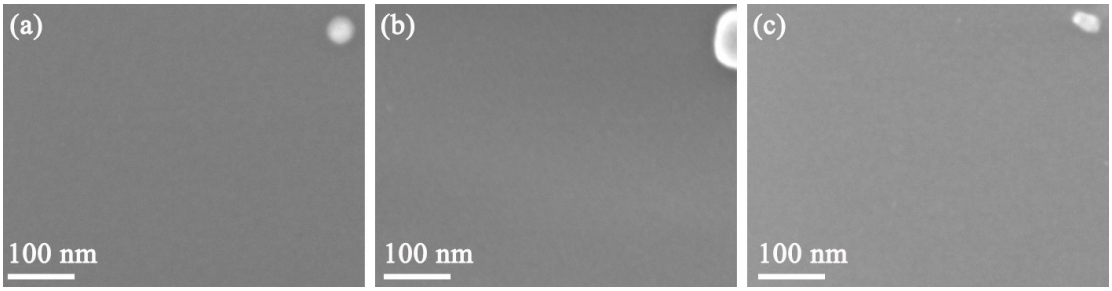

Fig. S5 SEM image of Ti-Cys hybrid films deposited at 135 °C (a) long-term stored by vacuum-packing, (b) placed in open air for 1 month, and (c) immersed in deionized water for 6 h.

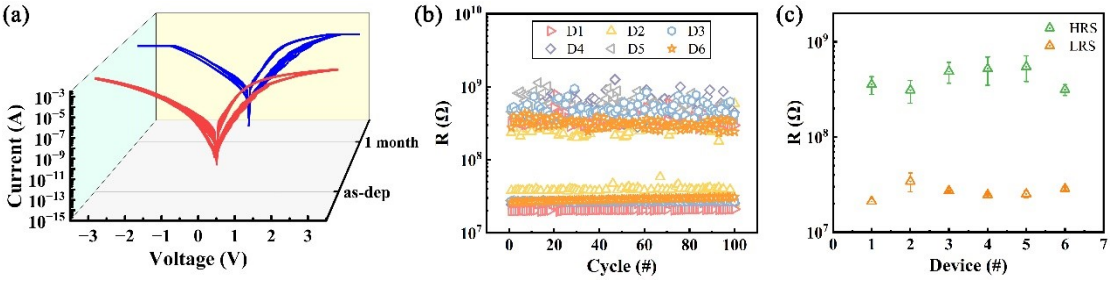

Fig. S6 (a) Waterfall illustration of I–V curves from 100 times tests before and after a month. (b) Endurance of six device cells for 100 switching cycles. (c) HRS and LRS distribution of six device cells from (b).

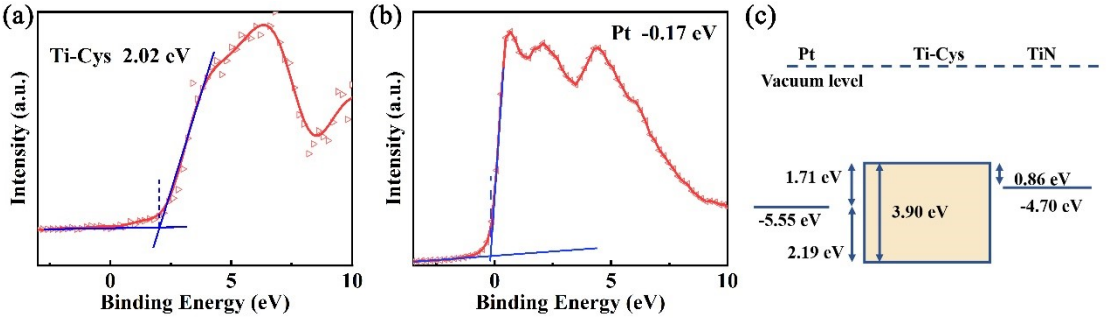

Fig. S7 Valence band spectra of (a)Ti-Cys and (b) Pt. (c) Energy band alignment of the hybrid thin film device of Pt/Ti-Cys/TiN by experimental measurements.

According to thermionic emission model, the current across a Schottky junction exhibits a specific voltage dependence. The standard Schottky emission equation is expressed as

$$I = AA^{*}T^{2}\left(exp\frac{-e\varphi_b}{kT}\right)\left(exp\frac{eV}{nkT}-1\right) \quad \text{(S1)}$$

where A is the contact area, A^* is the Richardson constant, T is the absolute temperature, ϕ_b is the effective Schottky barrier height (SBH), V is the applied bias, e is the unit charge, k is the Boltzmann constant, and n is the diode ideality factor.

To quantify the band alignment of the Pt/Ti-Cys junction, temperature-dependent I – V measurements were carried out. As shown in Figure S8(a), the junction current increases with temperature, rising from 298 K to 318 K. To determine the barrier height, Equation (S1) is transformed into the Arrhenius form

$$ln\left(\frac{I}{T^2}\right) \propto \left(\frac{-e\varphi_b}{k}\right)\left(\frac{1}{T}\right) \quad \text{(S2)}$$

Figure S8(b) displays the Arrhenius plots of $\ln(I/T^2)$ with respect to 1000/T at applied voltages of −0.05, −0.1, −0.15, −0.2, and −0.25 V. The resulting curves are linear for each bias, allowing us to extract the values of ϕ_b from the slopes of these linear plots. Figure S8(c) presents the barrier height values as a function of the applied bias. For our devices, the barrier height ϕ_b is approximately 1.86 eV at zero external bias, which is consistent with the value of 1.71 eV from energy band diagram in Figure S7c.

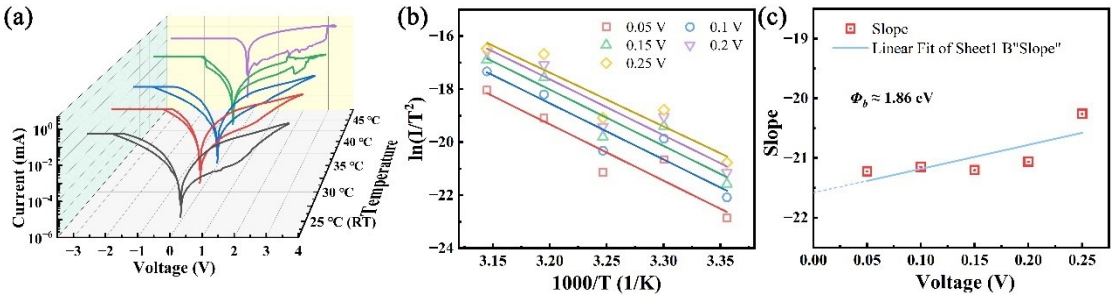

Fig. S8 (a) Waterfall illustration of I-V curves of the Pt/Ti-Cys/TiN hybrid film devices at different temperatures, ranging from 298 K to 318 K. (b) Plots of $\ln(I/T^2)$ versus $1000/T$ at various applied voltages. (c) Values of φ_b plotted with respect to the applied voltage.

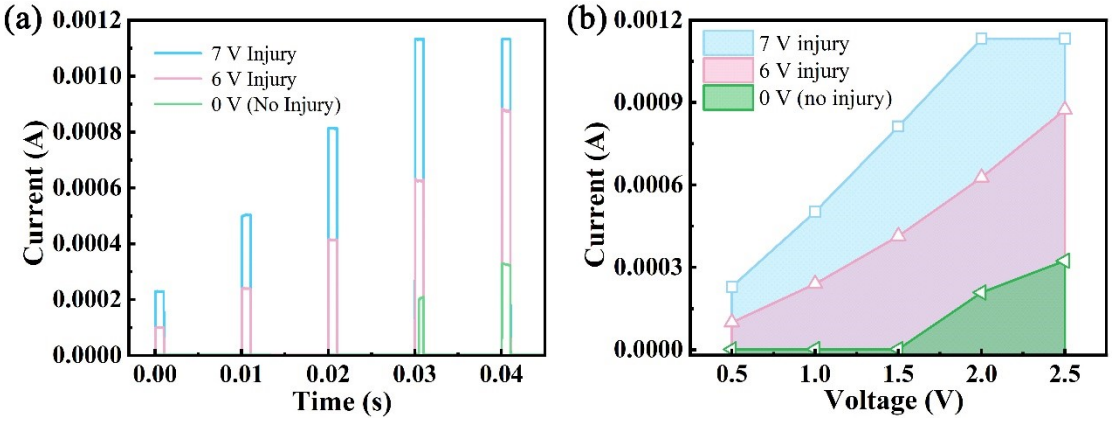

Fig. S9 (a) Output currents at 2 ms voltage pulses with different amplitudes (0.5, 1, 1.5, 2, 2.5, and 3 V) after different injury pulses (7 V– blue, 6 V– pink, 0 V– green/no injury for 10 ms). (b) Corresponding maximum output currents at different pulse amplitudes in linear scale.

Table S2 Comparison of our hybrid memristive artificial nociceptor and other materials as functional layer.

Materials stacks	Deposition Method	Functional Layer Thickness	Endurance	Nociceptor function	ref
Pt/ZrO_2/IGZO/TiN	Magnetron sputtering	8 nm	300	threshold, inadaptation, allodynia and hyperalgesia	1
Pt/TiO_2 nanobelts/Pt	Hydrothermal process	15-50 nm	80	threshold, inadaptation, relaxation, allodynia and hyperalgesia	2
Al/POT2T/$MAPbBr_3$/NiO_x/ITO	Spin-coating	260 nm	-	threshold, relaxation, allodynia and hyperalgesia	3
n-Si/VO_2/Au-coated probes	Thermal oxidation	142 nm	>100	threshold, relaxation, allodynia and hyperalgesia	4
Au/IZO/chitosan/IZO/Au	Spin-coating/ Magnetron sputtering	15 μm	-	threshold, relaxation, allodynia and hyperalgesia	5
Pt/Ti-Cys/TiN	MLD	10 nm	$>10^4$	threshold, inadaptation, relaxation, allodynia and hyperalgesia	This Work

References

1. X. Chen, Y. Jin, Z. Tao, L. Jiang, X. Wu, Y. Xiao, B. Jiang, X. Wen, J. Zhang, M. Zhu and C. Ye, *IEEE Trans. Electron Devices*, 2023, **70**, 1001-1005.
2. M. Xiao, D. Shen, M. H. Futscher, B. Ehrler, K. P. Musselman, W. W. Duley and Y. N.

Zhou, *Adv. Electron. Mater.*, 2020, **6**, 1900595.

3. R. A. John, N. Yantara, S. E. Ng, M. I. B. Patdillah, M. R. Kulkarni, N. F. Jamaludin, J. Basu, Ankit, S. G. Mhaisalkar, A. Basu and N. Mathews, *Adv. Mater.*, 2021, **33**, 2007851.

4. M. Kumar, J.-Y. Park and H. Seo, *Small Methods*, 2021, **5**, 2100566.

5. S. Jiang, Y. He, R. Liu, C. Chen, L. Zhu, Y. Zhu, Y. Shi and Q. Wan, *IEEE Trans. Electron Devices*, 2021, **68**, 415-420.